CHEMISTRY OF MATERIALS

Article

pubs.acs.org/cm

Thermodynamics, Kinetics and Structural Evolution of ϵ-$LiVOPO_4$ over Multiple Lithium Intercalation

Yuh-Chieh Lin,[†,¶] Bohua Wen,[‡,¶] Kamila M. Wiaderek,[§,¶] Shawn Sallis,[∥] Hao Liu,[§] Saul H. Lapidus,[§] Olaf J. Borkiewicz,[§] Nicholas F. Quackenbush,[⊥] Natasha A. Chernova,[‡] Khim Karki,[‡,▽] Fredrick Omenya,[‡] Peter J. Chupas,[§] Louis F. J. Piper,[⊥,∥] M. Stanley Whittingham,[*,‡] Karena W. Chapman,[*,§] and Shyue Ping Ong[*,†]

[†]Department of NanoEngineering, University of California San Diego, 9500 Gilman Drive # 0448, La Jolla, California 92093, United States

[‡]NECCES, Binghamton University, Binghamton, New York 13902, United States

[§]X-ray Science Division, Advanced Photon Source, Argonne National Laboratory, Argonne, Illinois 60439, United States

[∥]Materials Science & Engineering, Binghamton University, Binghamton, New York 13902, United States

[⊥]Department of Physics, Applied Physics and Astronomy, Binghamton University, Binghamton, New York 13902, United States

[▽]Center for Functional Nanomaterials, Brookhaven National Laboratory, Upton, New York 11973, United States

Supporting Information

ABSTRACT: In this work, we demonstrate the stable cycling of more than one Li in solid-state-synthesized ϵ-$LiVOPO_4$ over more than 20 cycles for the first time. Using a combination of density functional theory (DFT) calculations, X-ray pair distribution function (PDF) analysis and X-ray absorption near edge structure (XANES) measurements, we present a comprehensive analysis of the thermodynamics, kinetics, and structural evolution of ϵ-Li_xVOPO_4 over the entire lithiation range. We identify two intermediate phases at x = 1.5 and 1.75 in the low-voltage regime using DFT calculations, and the computed and electrochemical voltage profiles are in excellent agreement. Operando PDF and EXAFS techniques show a reversible hysteretic change in the short (<2 Å) V—O bond lengths coupled with an irreversible extension of the long V—O bond (>2.4 Å) during low-voltage cycling. Hydrogen intercalation from electrolyte decomposition is a possible explanation for the ∼2.4 Å V—O bond and its irreversible extension. Finally, we show that ϵ-Li_xVOPO_4 is likely a pseudo-1D ionic diffuser with low electronic conductivity using DFT calculations, which suggests that nanosizing and carbon coating is necessary to achieve good electrochemical performance in this material.

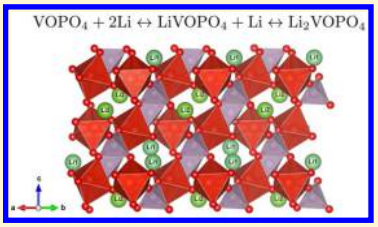

INTRODUCTION

The rechargeable lithium-ion (Li-ion) battery[1−4] has become a dominant form of energy storage for the modern age. However, the energy densities, both gravimetric and volumetric, of today's Li-ion batteries are still far below that necessary to displace gasoline combustion engines. For example, the capacities of the layered $LiMO_2$ cathodes,[3] which have the highest theoretical energy density of current commercial cathodes, are capped at around 180 mAh g^{-1}, leading to corresponding calculated energy densities of around 1 kWh kg^{-1} and 3 kWh L^{-1}.[5] Other commercial cathodes have significantly lower energy densities, e.g., the high rate $LiFePO_4$[4] cathode has maximum theoretical energy densities of 587 Wh kg^{-1} and 2 kWh L^{-1}. In commercial cells, the energy densities are even lower, the best not exceeding 250 Wh kg^{-1} and 0.6 kWh L^{-1}.[6]

The energy density of a cathode is given by the product of its voltage and its capacity. A push for high voltage reactions has motivated the strong interest in phosphate-based cathodes such as $LiFePO_4$ and $LiMnPO_4$ with increased voltage (relative to simple oxides) associated with the inductive effect of the PO_4^{3-} polyanion.[4] The majority of commercial cathodes today operate on a single redox per transition metal on average, which ultimately limits capacities. A potential path toward higher capacities is to develop multielectron cathodes that reversibly cycle more than one electron per transition metal. Given the fact that current organic carbonate electrolytes can only support voltages up to around 4.5 V,[7] a previous high-throughput first-principles analysis[8] has shown that only V and Mo have reasonable average voltages across multiple redox couples ($V^{3+} \rightarrow V^{5+}$ and $Mo^{3+} \rightarrow Mo^{6+}$) to be practical multielectron phosphate-based cathodes.

The vanadyl phosphates with formula $VOPO_4$ are an interesting class of multielectron cathode materials that utilize the $V^{3+} \leftrightarrow V^{4+} \leftrightarrow V^{5+}$ couple. Indeed, insertion of two Li into the ϵ polymorph of $VOPO_4$ has been demonstrated.[9−12] However, there are distinct differences between the insertion/deinsertion behaviors of the first and second Li. The insertion of the first Li at ∼3−4.5 V[13] has been shown to be relatively

Received: December 17, 2015
Revised: February 26, 2016
Published: February 29, 2016

DOI: 10.1021/acs.chemmater.5b04880
Chem. Mater. 2016, 28, 1794−1805

facile and reversible with small overpotential. The insertion of the second Li, on the other hand, is associated with a much larger overpotential.[10] Although previous studies conclusively demonstrate that the first Li insertion takes place via a two-phase reaction, there is disagreement on the nature of the second Li insertion. Some works suggest the existence of several intermediate phases at ~ $Li_{1.5}VOPO_4$ and $Li_{1.75}VOPO_4$,[10,12] whereas Harrison et al.[11] suggest a single-phase region between $Li_{1.5}VOPO_4$ and Li_2VOPO_4.

In ε-Li_xVOPO_4, the VO_6 polyhedra share corners to form one-dimensional (1D) chains (see Figure 1). These chains are

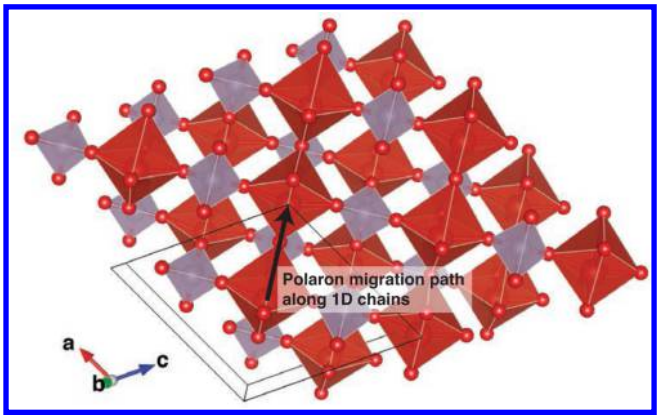

Figure 1. Crystal structure of $VOPO_4$, showing polaron migration along 1D VO_6 chains.

bridged by PO_4. All V ions are symmetrically equivalent in $VOPO_4$ (*Cc* spacegroup), whereas alternating V ions along the 1D chains are symmetrically inequivalent in $LiVOPO_4$ and Li_2VOPO_4 ($P\bar{1}$ space group). It is only recently that a structure for the Li_2VOPO_4 end member has been proposed for a chemically lithated sample.[11,12] For historical reasons, the singly lithiated phase of ε-$VOPO_4$ is known as α-$LiVOPO_4$ based on the order of discovery. For the sake of clarity, we will adopt the convention proposed by Whittingham et al.[5] and refer to all lithiated members of ε-$VOPO_4$ with the ε prefix. Also, unless otherwise stated, formulas given without a prefix refer to the ε phase.

In this work, we demonstrate the stable cycling of more than one Li in solid-state-synthesized ε-$LiVOPO_4$ for more than 20 cycles for the first time. In contrast to previous work, we apply an integrated approach combining density functional theory (DFT) calculations, operando X-ray pair distribution function (PDF) and diffraction analysis, and extended X-ray absorption fine structure (EXAFS) measurements to elucidate the thermodynamics, kinetics and structural evolution of ε-Li_xVOPO_4 over multiple Li intercalation. The main accomplishments include the identification of candidate stable structures for $Li_{1.5}VOPO_4$ and $Li_{1.75}VOPO_4$, the observation and explanation of a hysteretic V—O bond length evolution during low voltage cycling, and a discussion of the phase stability and ionic and electronic conductivity considerations in achieving good electrochemical performance in this material.

EXPERIMENTAL METHODS

Synthesis. ε-$LiVOPO_4$ was prepared via solid state synthesis. Stoichiometric amounts of NH_4VO_3 (Aldrich, 99%), Li_2CO_3 (Fisher Scientific, ≥ 99%), and $NH_4H_2PO_4$ (Sigma-Aldrich, ≥ 99.99%) were mixed with acetone in a planetary ball mill for 4h. The isolated solid mixture was pressed into pellets and heated in argon atmosphere at 300 °C for 5h and then at 750 °C for 10h. The structure of the as-prepared material was verified using powder diffraction analysis and transmission electron microscopy (TEM) (see Supporting Information, SI). Nanocomposite ε-$LiVOPO_4$ was prepared by high energy ball-milling the as-synthesized material with Super P carbon black and PVDF (poly(vinylidene fluoride)) in a weight ratio of 75:15:10.

Electrochemistry. Electrodes were fabricated by casting the nanocomposite onto Al foil. Electrodes with 5−6 mg of active material of area 1.2 cm^2 were assembled into 2325-type coin cells with a Celgard 2400 separator (Hoechst Celanese), lithium metal foil (Aldrich) and liquid electrolyte (1 M $LiPF_6$ in 1:1 ethylene carbonate: dimethylcarbonate, EC:DMC). The thickness of the electrode was ~40 μm. The electrochemical properties were investigated using VMP multichannel potentiostat (Bio-Logic). Cells were cycled galvanostatically at C/50 (~0.01 mA/cm^2) in the high voltage (3.0−4.5 V), low-voltage (1.5−3.5 V) and whole voltage (1.6−4.5 V) regimes. Cells were also cycled at C/20 (~0.02 mA/cm^2) over the whole voltage range. The kinetics in the high- and low-voltage regimes were explored using GITT testing by applying C/50 current for 1.5 h followed by resting for 100 h at high voltage or 24 h at low voltage.

Operando Pair Distribution Function (PDF) and Diffraction Analysis. Operando X-ray scattering data were collected for ε-$LiVOPO_4$ based pellet electrodes within the AMPIX electrochemical cell.[14] 13 mm-diameter electrode pellets of 120−180 μm thick were prepared from the $LiVOPO_4$ nanocomposite as described previously. The electrode pellets were assembled into an electrochemical cell in an Ar-atmosphere glovebox with a glass fiber separator (Whatman GF/A), Li metal foil and liquid electrolyte (1 M $LiPF_6$ in 1:1 EC:DMC, from BASF). The cell was cycled galvanostatically at a constant current of 5 mA g^{-1}, in the voltage range of 3.5 V to 1.6 V to 3.5 V ($LiVOPO_4$ to Li_2VOPO_4 to $LiVOPO_4$).

X-ray scattering data were collected in 3 min exposures at beamline 11-ID-B at the Advanced Photon Source, Argonne National Laboratory, using high energy X-rays (~58 keV, λ = 0.2114 Å) in combination with a large amorphous-silicon based area detector (PerkinElmer). Data were collected at 15 min intervals alternating between PDF and pXRD optimized configurations (equivalent to 0.015 Li intervals for each) during the first lithiation and delithiation cycle. Total scattering data suitable for PDF analysis were collected to high values of momentum transfer (Q_{max} ~ 22 Å).[15,16] Diffraction data optimized for improved 2θ resolution were collected using a long sample-to-detector distance. The scattering images were reduced to one-dimensional data using fit2d.[17]

The large Q-range total scattering data were corrected for background scattering, Compton scattering and detector effects within pdfgetX2 and Fourier transformed to get $G(r)$, the PDF.[18] Structure models were refined against the PDF data and the corresponding partial pair contributions to the PDFs calculated within PDFgui.[19] A spherical particle envelope parameter was used to model the particle size and/or length scale of ordering. The intensity and position of peaks corresponding to the V═O/P—O bond (ca. 2.0 Å) and the V—O bond (ca. 2.5 Å) were quantified by fitting Gaussian functions within fityk.[20] The evolution of the crystallographic lattice dimensions and average structure was evaluated based on Rietveld refinement of the powder diffraction data within TOPAS.

X-ray Absorption Spectroscopy. X-ray absorption data were collected for Li_xVOPO_4 electrodes recovered at different states of charge at beamline 9-BM-B of the Advanced Photon Source, Argonne National Laboratory. The V k-edge (E = 5.463 keV) XANES and EXAFS spectra were acquired in transmission mode. A k-range of 1−7 $Å^{-1}$ was used in the Fourier transformed R-space functions. Data were processed in Athena and Artemis from the Demeter software package version 0.9.21.[21]

COMPUTATIONAL METHODS

All density functional theory (DFT) calculations were performed using the Vienna Ab initio Simulation Package (VASP)[22] within the projector augmented-wave approach.[23] Appropriate functionals and parameters for each analysis were selected based on accuracy and computational cost considerations. Initial candidate structures for ε-

DOI: 10.1021/acs.chemmater.5b04880
Chem. Mater. 2016, 28, 1794−1805

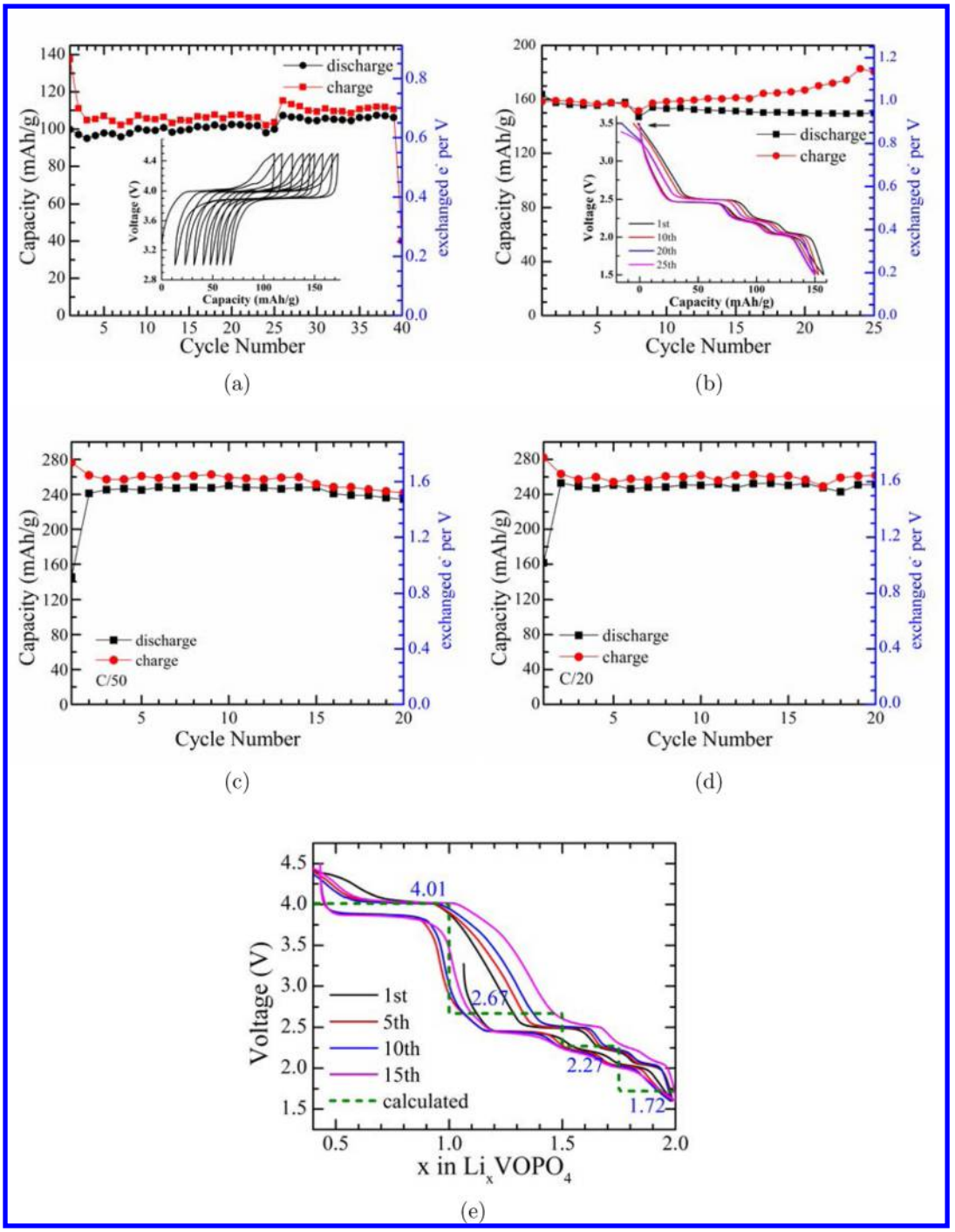

Figure 2. Galvanostatic charge−discharge cycling of ε-LiVOPO$_4$: (a) high voltage cycling within 3−4.5 V (C/50) and (b) low voltage cycling in the range of 1.5−3.5 V (C/50). Two lithium cycling from 1.6 to 4.5 V (c) at C/50 and (d) C/20 (1C = 159 mA/g); (e) Comparison between experimental voltage curve at 50C and HSE calculated voltage profile.

$VOPO_4$, $LiVOPO_4$ and Li_2VOPO_4 were obtained from the experimental literature.[12,24] Candidate intermediate structures Li_xVOPO_4 (x = 0.25, 0.5, 0.75, 1.25, 1.5 and 1.75) were derived by partially delithiating $LiVOPO_4$ or Li_2VOPO_4 and carrying out an enumeration[25] of all symmetrically distinct orderings (see SI for details). All analyses were performed using the Python Materials Genomics (pymatgen) library.[26]

Phase Equilibria and Voltage Profile. The energies of all Li_xVOPO_4 phases were calculated using the Perdew−Burke−Ernzerhof (PBE) generalized-gradient approximation[27] functional with the application of an effective Hubbard U[28−30] of 3.25 eV for vanadium (GGA+U). The calculation parameters were based on the parameters used in the Materials Project.[31] The key parameters are a plane wave energy cutoff of 520 eV and k-point density of at least 1000/(number of atoms in unit cell). All calculations were spin-polarized starting from a high-spin ferromagnetic configuration as a previous first-principles study has shown that the magnetic ordering has a small effect on the relative total energies in this system.[32] We assessed the phase stability of Li_xVOPO_4 by constructing the pseudobinary $VOPO_4$−Li_2VOPO_4 phase diagram, as well as the full Li−V−P−O quarternary phase diagram with data from the Materials Project.[33,34] The voltage profile was then constructed from the stable orderings.[35] We also performed energy calculations using the screened hybrid Heyd−Scuseria−Ernzerhof (HSE) functional[36,37] to obtain

DOI: 10.1021/acs.chemmater.5b04880
Chem. Mater. 2016, 28, 1794−1805

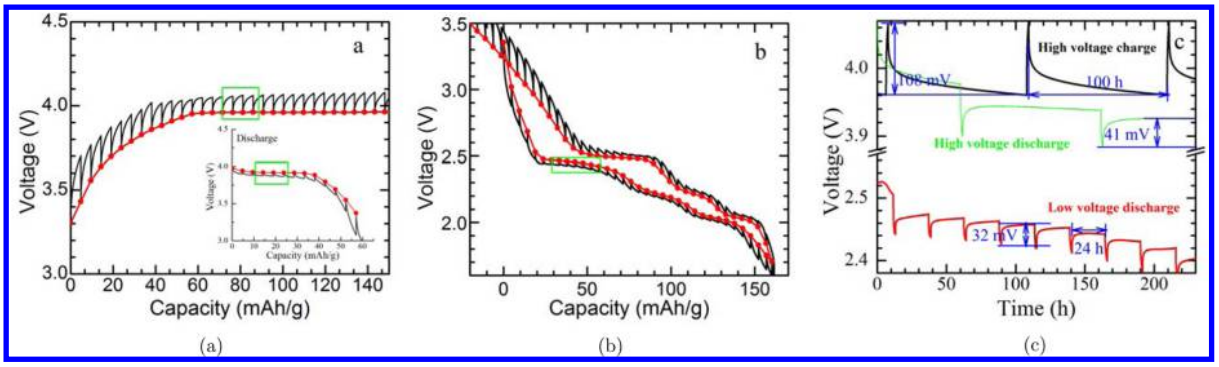

Figure 3. GITT capacity-voltage profiles of ε-$LiVOPO_4$ in the (a) high voltage and (b) low-voltage domains. (c) Voltage vs time graph of the magnified marked region. C/50 current was applied for 1.5 h before rest; 24 h relaxing for low voltage and 100 h for high voltage.

more accurate structural parameters, electronic structure, and voltages. Given the much greater computational expense of HSE calculations, these calculations were limited to only the lowest energy orderings at each composition obtained from the GGA+U calculations.

Vacancy Migration Barriers. Activation barriers for vacancy (v_{Li^+}, a lower case v is used to denote a vacancy) migration in $LiVOPO_4$ were calculated using the climbing image nudged elastic band method (CI-NEB).[38,39] To avoid ambiguity regarding the localization of electrons, the standard PBE GGA functional (without application of the Hubbard U) was used, in line with the well-established practice in the literature.[40] The CI-NEB calculations were carried out using a $2 \times 2 \times 2$ supercell with formula $Li_{31}V_{32}O_{32}P_{32}O_{128}$ (32 formula units with a Li vacancy) to minimize the interactions between periodic images. A Γ $1 \times 1 \times 1$ k-point grid was used, and each image is relaxed until the forces on each atom are less than 0.02 eV/Å. Investigation of vacancy migration in Li_2VOPO_4 was not carried out as the introduction of a vacancy leads to a substantial rearrangement of Li atoms in the crystal due to the large number of Li atoms in the unit cell.

Electronic Conductivity. The electronic conductivity of Li_xVOPO_4 was assessed by calculating the band gaps and small polaron migration barriers using the HSE functional.[41,42] A slow moving electron or hole in a dielectric crystal induces a local lattice distortion, which acts as a potential well that causes the charge carrier to become self-trapped. The quasiparticle formed by the charge carrier and its self-induced distortion is called a small polaron if the range of the lattice distortion is of the order of the lattice constant. In this work, we adopted the same methodology used previously by one of the coauthors to study of polarons in the $LiMPO_4$ (M = Fe, Mn) olivines.[43] In Li_xVOPO_4, we can assume that electron transfer is confined within each 1D chain with no charge transfer through the PO_4 polyanions. The maximum barrier calculated for the charge to move from one V atom to its nearest periodic image along the chain is an upper limit for the migration barrier. In $VOPO_4$, polaronic charge carriers are electrons on V^{5+} sites. In $LiVOPO_4$, polaron charge carriers can either be holes or electrons on V^{4+}, forming a localized V^{5+} or V^{3+} state, respectively. In Li_2VOPO_4, it is assumed that polaronic charge carriers are holes on V^{3+} sites given the fact that further reduction of V beyond a two-electron process has thus far not been demonstrated. The polaron migration barriers were calculated using a ferromagnetic structure. Supercells containing 16 formula units ($2 \times 1 \times 2$ for $VOPO_4$ and $2 \times 2 \times 1$ for $LiVOPO_4$ and Li_2VOPO_4) were used to minimize the interaction between periodic images while keeping computational costs at a reasonable level. The HSE functional was used for the polaron calculations. Similar to the $LiMnPO_4$ olivine studied previously,[43] we found that a polaron cannot be localized in Li_xVOPO_4 with the GGA+U functional, likely due to the strong hybridization between V and O. A fairly tight energy convergence criteria of 0.001 eV was used, with a minimal Γ $1 \times 1 \times 1$ k-point grid.

RESULTS

Electrochemistry of ε-$LiVOPO_4$. The first effort of this work was to optimize the solid state synthesis of ε-$LiVOPO_4$ as the method originally proposed by Ateba Mba et al. was for $LiVOPO_4F$.[44] NH_4VO_3 was used as a V^{5+} precursor, and pure ε-$LiVOPO_4$ was readily obtained at 750 °C. The high resolution X-ray diffraction pattern and TEM image of the as-synthesized and high energy ball-milled ε-$LiVOPO_4$ are given in Figure S1 of the SI. After ball milling with super P carbon black, the micron-size as-synthesized $LiVOPO_4$ particles are fragmented, forming an agglomerate of smaller multigrained particles with a thin layer of carbon (thickness ~2 nm) on the surface. The resulting clusters are less than 100 nm in size (Figure S1e of the SI).

Figure 2a and b show the galvanostatic cycling of ball milled ε-$LiVOPO_4$ in the high- (3.0–4.5 V) and low-voltage (1.5–3.5 V) domains, respectively. The high-voltage $V^{4+/5+}$ plateau consistently delivers a reversible capacity of ~105 mAh/g for up to 35 cycles, which corresponds to ~0.65 Li. The charge–discharge profiles are similar after 25 cycles (inset of Figure 2a), but the initial charge curve is different. Electrolyte decomposition above 4.2 V leads to the initial capacity loss, as seen in Figure 2a. These results are comparable with most previous reports on the cycling of $VOPO_4$ and $LiVOPO_4$.[11,13,45] In the low-voltage region, the capacity from the $V^{3+/4+}$ couple is close to 1 Li and stable for 25 cycles (Figure 2b). The discharge–charge profiles with steps are in agreement with many reports, suggesting the existence of intermediate phases at 1.5 and 1.75Li.[11,12,45] The inset of Figure 2b compares the curves of the 1st, 10th, 20th, and 25th cycles.

The cells were also cycled over the whole voltage range (1.6–4.5 V), as shown in Figure 2c and d. A high capacity of ~240 mAh/g can be achieved for up to 20 cycles, corresponding to 1.65 Li with little dependence of capacity on the rate. Both plateaus deliver a similar capacity as when cycled separately. From Figure 2e, we see that the profiles of C/50 cycling evolve from step-like to more slope-like, especially at low-voltage, and the difference between voltage plateaus increases progressively, suggesting changes in the local structure. At C/20, this effect is more pronounced. These observations clearly suggest inherent kinetic limitations, particularly in the high-voltage regime. Indeed, sluggish kinetics in the high-voltage regime have been recently considered responsible for pronounced Li gradients and reduced capacity in hydrothermally synthesized ε-$VOPO_4$.[46] Overall, the electrochemical performance is consistent with previous reports, indicating that it is easier to intercalate Li into than to remove Li from ε-$LiVOPO_4$. This is the first time cycling of multiple Li^+ in phosphates has been achieved for up to 20 cycles.

DOI: 10.1021/acs.chemmater.5b04880
Chem. Mater. 2016, 28, 1794–1805

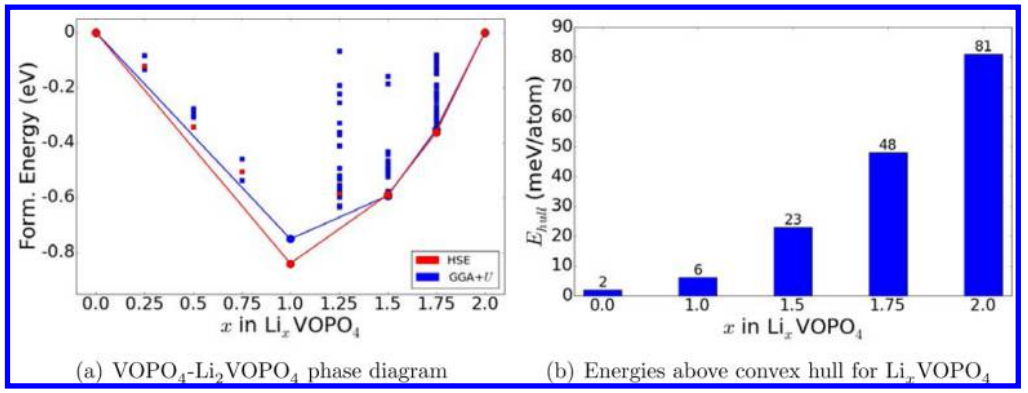

Figure 4. (a) Calculated pseudobinary $VOPO_4$–Li_2VOPO_4 phase diagram using the HSE (blue) and GGA+*U* (green) functionals. Squares, unstable structures; circles, stable structures; lines, convex hull. (b) Calculated energies above the convex hull for stable orderings in the pseudobinary $VOPO_4$–Li_2VOPO_4 system in GGA+*U*. The convex hull is calculated with respect to all phases in the full Li–V–P–O calculated phase diagram.

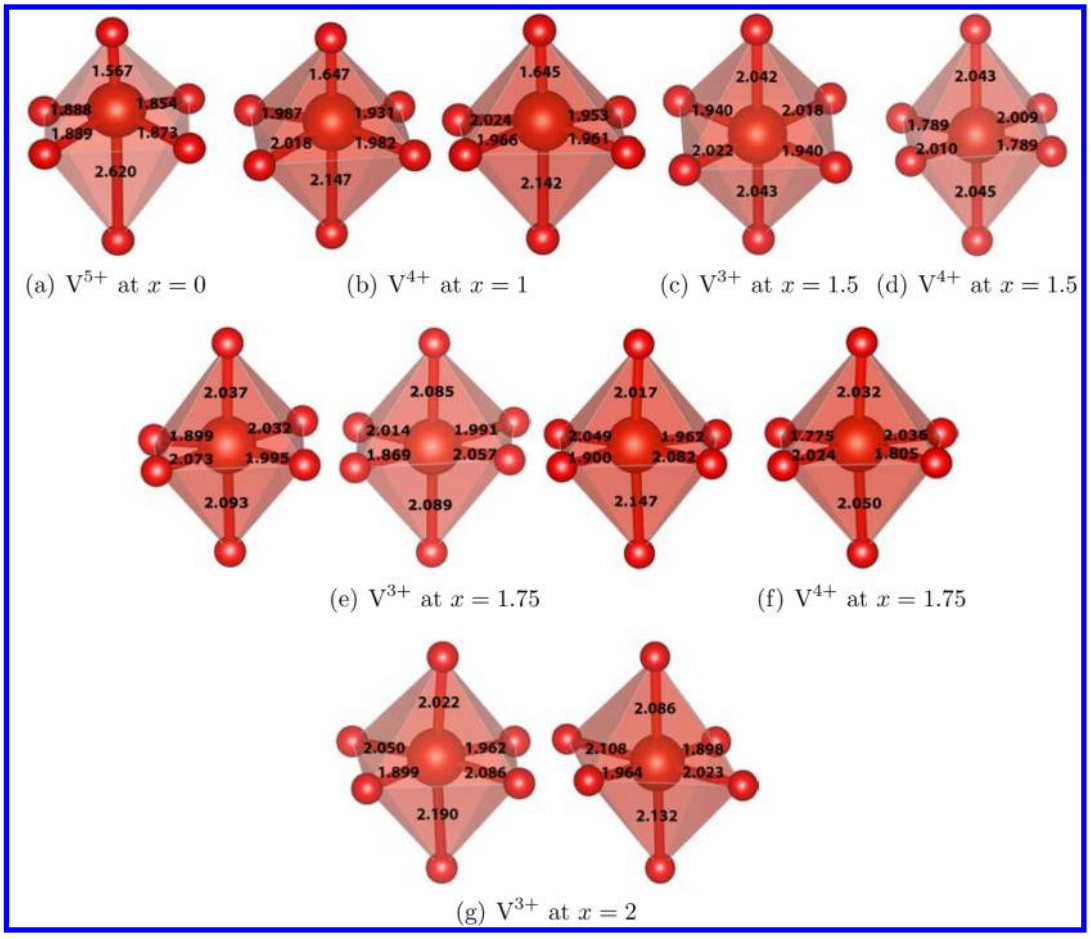

Figure 5. Symmetrically distinct VO_6 local environments in Li_xVOPO_4 from structures relaxed using HSE calculations. Large sphere: vanadium ion. Small sphere: oxygen ion.

The kinetics in the high and low voltage regimes were explored using GITT testing. Figure 3a and b plot the capacity-voltage graph in the high- and low-voltage regions respectively, which is similar to the constant rate charge–discharge curves. The overpotentials and relaxation of the reactions in the high- and low-voltage plateaus in the green box are shown in Figure 3c. At low voltage, the discharge overpotential is ~32 mV, three times less than the high-voltage charge process (~108 mV), and is comparable to the high-voltage discharge process (~41 mV). This observation implies the intercalation process at high-voltage has to overcome a higher energy barrier than at low-voltage, which restricts the amount of lithium that can be reversibly extracted. Electrolyte decomposition during high-voltage charging may further limit the amount of Li extracted. The transitions between V^{3+}/V^{4+} and V^{4+}/V^{5+}, where more energy is needed for nucleation, always manifest the highest overpotentials. The voltage at low plateau region is stable in 24 h, and 100 h relaxation is insufficient for the high-voltage reaction to reach equilibrium. These observations conclusively demonstrate the faster kinetics reaction at the low-voltage region, indicating that it is easier to intercalate Li into than to remove Li from ϵ-$LiVOPO_4$.

DOI: 10.1021/acs.chemmater.5b04880
Chem. Mater. 2016, 28, 1794–1805

Figure 4a shows the 0 K pseudobinary $VOPO_4$–Li_2VOPO_4 phase diagram calculated using the GGA+U and screened hybrid HSE functionals. For $0 \leq x \leq 1$, the phase diagram predicts that there are no stable intermediate phases, consistent with the two-phase behavior observed in our high-voltage cycling (Figure 2a) and previous results.[11,12,32,47] Two stable intermediate phases are predicted at $x = 1.5$ and 1.75 for $1 \leq x \leq 2$, which is again consistent with the three plateaus observed during low voltage cycling (Figure 2b). We find that the average voltages calculated using the HSE functional are in much better agreement with experiments compared to those calculated using GGA+U, possibly due to a better description of the strongly hybridized V—O bonds and the fact that the Hubbard U value is a fitted average (see SI for details). Overall, we find that our computed HSE voltage profile is in fairly good agreement with the electrochemically measured profile (see Figure 2e) and values in the literature (see Table S4 of the SI). This agreement gives us confidence that the intermediate structures obtained in our approach are reasonably close to the true ground state structures.

Figure 4b shows the calculated GGA+U E_{hull} relative to all known Li–V–P–O phases for the stable orderings in the $VOPO_4$–Li_2VOPO_4 pseudobinary. The E_{hull} is an estimate of the thermodynamic stability of a phase; stable phases have an E_{hull} of 0, whereas increasing E_{hull} indicates decreasing thermodynamic stability. We observe that although the E_{hull} remains relatively low up to $x = 1$, it rapidly increases upon further lithiation, which indicates that highly lithiated Li_xVOPO_4 phases are thermodynamically unstable. All highly lithiated Li_xVOPO_4 are predicted to be unstable with respect to a linear combination of $Li_3V_2(PO_4)_3$, Li_3PO_4, and vanadium oxides.

Local V Structure. Figure 5 shows the symmetrically distinct VO_6 environments extracted from the stable HSE-relaxed structures. In general, the HSE lattice parameters are in excellent agreement with the experimental lattice parameters[12] (see Table S1 in the SI). As the atomic positions of the intermediate $Li_{1.5}VOPO_4$ and $Li_{1.75}VOPO_4$ phases have not been reported previously, the DFT relaxed positions are given in Tables S2 and S3 in the SI. In agreement with previous findings,[11,12] both the predicted $Li_{1.5}VOPO_4$ and $Li_{1.75}VOPO_4$ structures have $P\bar{1}$ symmetry, though the lowest energy $Li_{1.75}VOPO_4$ structure is a supercell that is twice the size of the primitive cell of Li_2VOPO_4. It is, however, likely that Li disorder is present in $Li_{1.75}VOPO_4$ given the presence of multiple orderings that are close in energy (and hence, potentially thermodynamically accessible at finite temperatures) to the ground-state ordering (see Figure 4a).

The calculated models of all intermediates were compared to the data collected for the ex-situ samples recovered from coin cells from electrochemical cycling and to the selected points of the operando data. Refinement of the lattice parameters (Figure S3 in the SI) yielded a good fit for the long-range structure (beyond 15 Å), though significant deviations in the local structure remain. Further refinements of oxygen coordinates yielded excellent fits over all length scales (Figure 6).

Partial pair contributions to the PDFs were calculated based on the refined model to identify the atom–atom pairs associated with different features in the experimental data (see Figure S4 in the SI). The V has an asymmetric coordination environment, with one short V—O bond (1.62 Å) and five longer V—O bonds (~1.99 Å). In the total PDF, the short V—O bond at ~1.6 Å overlaps with the contribution

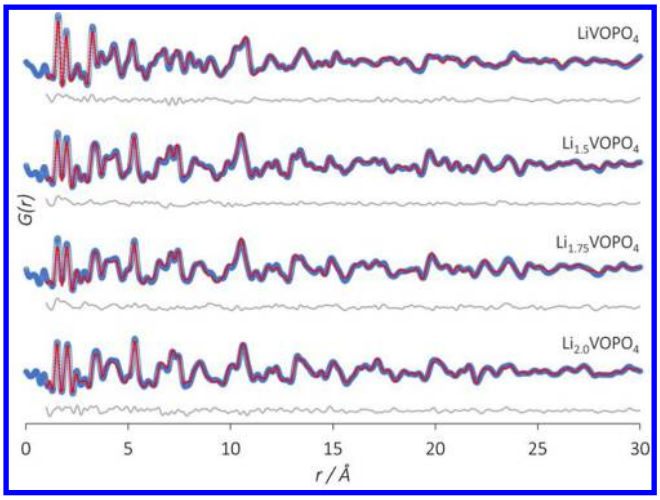

Figure 6. Refinements of all intermediates based on the HSE-relaxed structures, lattice parameters, and oxygen atomic positions.

from the P—O distance within the PO_4^{3-} anion. These bond lengths are in excellent agreement with the HSE-relaxed VO_6 environments for $LiVOPO_4$.

The operando PDF data, collected during lithiation and delithiation between $x = 1$ and $x = 2$, revealed marked changes in the local atomic structure and V coordination (Figure 7a). Continuous shifts in the 1.6 and 2.0 Å peak positions reflect changes in the average bond lengths, whereas the changes in peak areas correspond to changes in the average coordination number. Discontinuous changes were observed for the peak at ~3.3 Å, corresponding to the V(—O—)P distance. This likely reflects changes in the V—O—P angle associated with a relative rotations of the VO_6 and PO_4 polyhedra during the structural phase transitions. The changes in the local structure were quantified by fitting Gaussian functions to features in the PDFs up to 4 Å. Although the contributions from the P—O and short V—O bonds are not well resolved in the operando data, the PO_4 polyatomic anion geometry is not expected to change during cycling, so all changes in the feature at ca. 1.6 Å can be entirely attributed to changes in the V═O bond. The intensity and position of the feature associated with the P—O bond was fixed for the analysis.

More pronounced changes were observed for the V═O bond length compared to the V—O bond (Figure 7b). During the initial stage of reaction, corresponding to the transition between $LiVOPO_4$ and $Li_{1.5}VOPO_4$, the short terminal V═O bonds elongate rapidly by 0.15 Å, whereas longer V—O interactions increase only by 0.008 Å. The elongation of the V═O bond is accompanied by a decrease in the relative intensity of this peak and a small, but not equivalent, increase in the intensity of the V—O feature at 2.0 Å. Once the V═O correlations are effectively eliminated, the longer V—O bond grows more rapidly. The average V—O bond lengthens most rapidly between $Li_{1.5}VOPO_4$ and $Li_{1.75}VOPO_4$ (2.014 Å to 2.026 Å), with slower changes again between $Li_{1.75}VOPO_4$ and Li_2VOPO_4 (2.026 Å to 2.034 Å). The intensity weighted average of V—O distance changes more continuously. The overall changes in V—O distance are reversed upon delithiation. These observations are consistent between the PDF measurements and the DFT computed structures (Figure 5).

Clear hysteresis is observed for the V—O features between lithiation and delithiation (Figure 8a). The V—O bond

DOI: 10.1021/acs.chemmater.5b04880
Chem. Mater. 2016, 28, 1794–1805

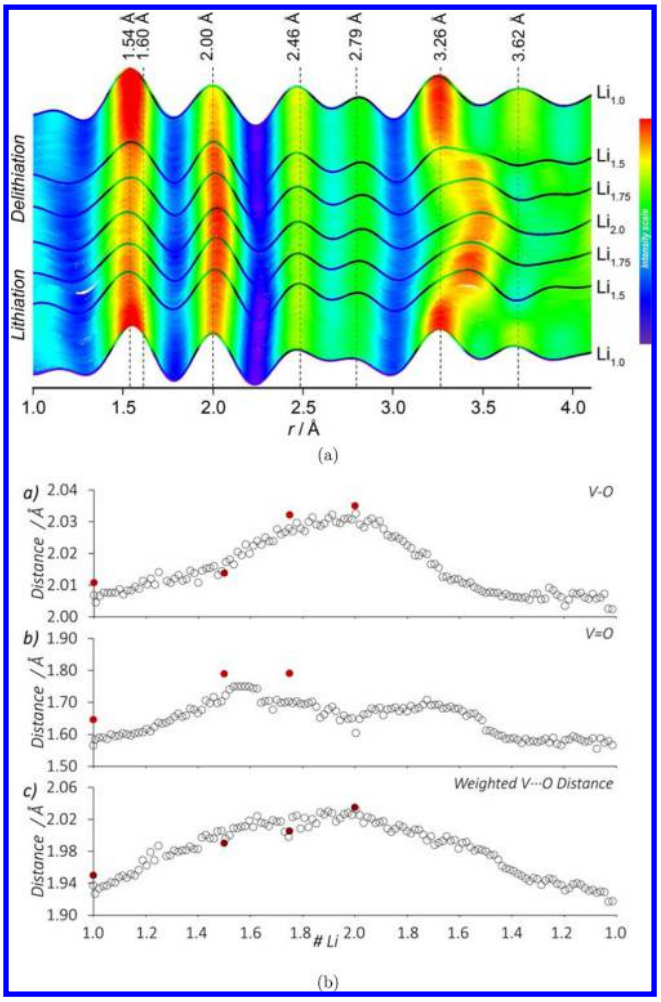

Figure 7. (a) Operando PDF data obtained during cycling of $LiVOPO_4$ in the range 3.5−1.6−3.5 V. (b) Peak positions corresponding to the V—O and V═O bonds, and the intensity-weighted average value. Experimental data, open markers; HSE calculated distances, red closed markers.

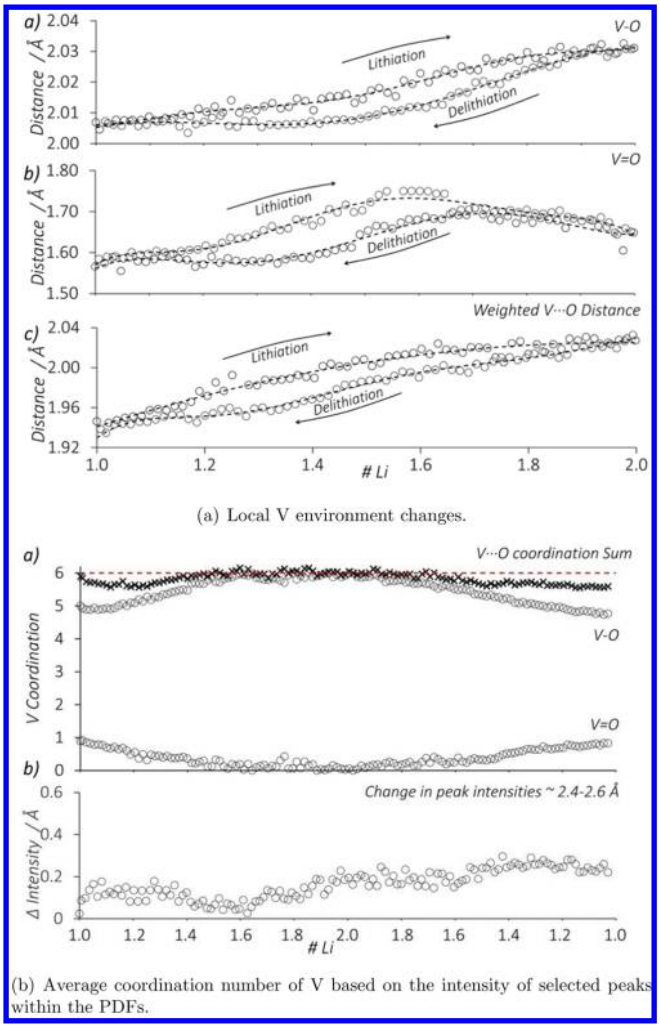

Figure 8. Changes in V—O bond lengths and coordination showing hysteresis during lithiation and delithiation.

contracts more rapidly during delithiation compared to the elongation during lithiation. Correspondingly, stable intermediates appear to form ∼0.1 Li earlier during delithiation than during lithiation ($Li_{1.6}VOPO_4$ vs $Li_{1.5}VOPO_4$) as is reflected by the relevant plateaus in the electrochemistry. The hysteresis within each V—O bond is noticeable throughout the entire composition range. The shorter V interactions exhibit large hysteresis associated with only the first $Li_{1.5-1.6}VOPO_4$ intermediate.

The V—O coordination number for V—O bonds of less than ∼2.2 Å drops during the reaction (Figure 8b), which reflects either under-coordination of V or the formation of a long ∼2.4 Å V—O bond. The initial V local environment has 1 short V═O and 5 longer V—O correlations on average. During the transformation from $LiVOPO_4$ to $Li_{1.5}VOPO_4$, the total intensity in the V—O features at 1.6 and 2.0 Å reduces from 6 to 5.5 O neighbors, suggesting that up to half of the V have an elongated V—O bond. This is supported by an increase in intensity for the features at 2.5 and 2.8 Å, which are primarily assigned to O—O distances. During charge, the V—O coordination drops to 5.5 beyond 1.75 Li, but this is not reversed by 1 Li.

The local V coordination environment for a set of ex-situ samples was determined via EXAFS. The Fourier transformed k^2 weighted data is plotted (offset for clarity) in Figure 9a. The peak around 1.5 Å is associated with the first coordination shell around the central absorbing atom. First coordination shell fits were performed using a model for the VO_6 octahedron, which included long and short apical bonds (created by displacing the central V along the z axis) as well as four equivalent equatorial bonds. Bond lengths were determined by fitting unique ΔR values for all scattering paths and all samples. Coordination number (N) and amplitude reduction (S_0^2) were taken to be constant. A single Debye−Waller factor (σ^2) and energy shift (E_0) were used for all scattering paths and samples. Consistent with the PDF analysis, we identify a short and equatorial V—O radial distance at ∼1.6 and 2.0 Å respectively. The presence of a long bond around 2.4−2.5 Å is also apparent from Figure 9c. The long bond length increases with increasing state of discharge and then recovers (with a clear overpotential) upon recharge. The observation of a long V—O bond length at ∼2.4 Å in our PDF and EXAFS measurements is consistent with previous EXAFS results by Allen et al.[45]

Ionic Conductivity. We investigated the migration barriers for v_{Li+} hopping in $LiVOPO_4$ using CI-NEB calculations. The unit cell of $LiVOPO_4$ contains two crystallographically distinct Li sites (labeled Li1 and Li2) that form percolating 1D chains,

DOI: 10.1021/acs.chemmater.5b04880
Chem. Mater. 2016, 28, 1794−1805

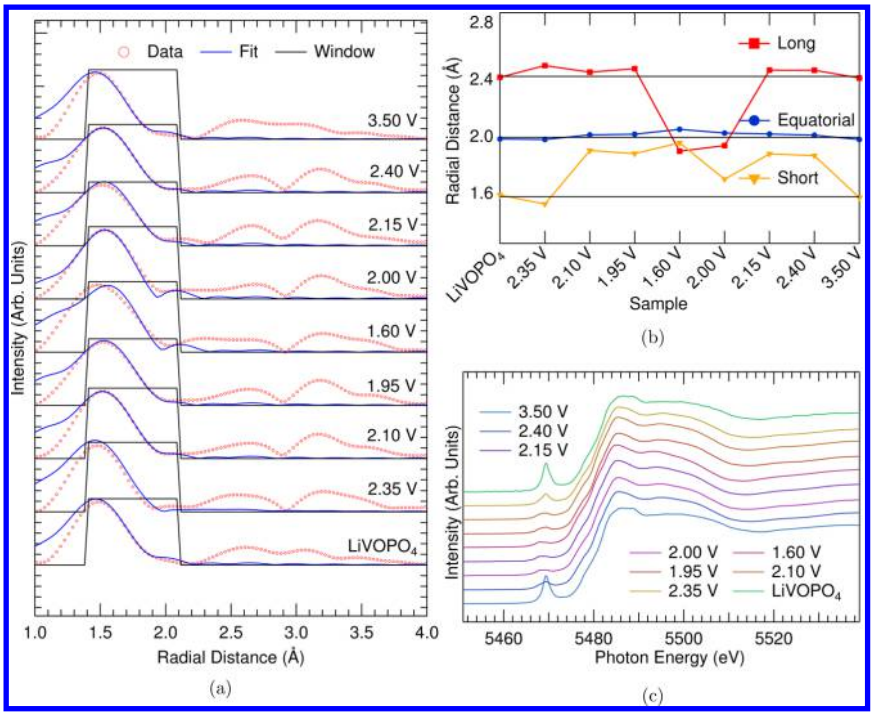

Figure 9. EXAFS analysis of ex-situ $LiVOPO_4$ cathodes at various states of charge. (a) First shell fits using an asymmetric model for the VO_6 octahedron including long and short apical bonds, and four equivalent equatorial bonds. (b) V—O bond lengths at different states of charge. (c) Normalized XANES spectra used for the fitting.

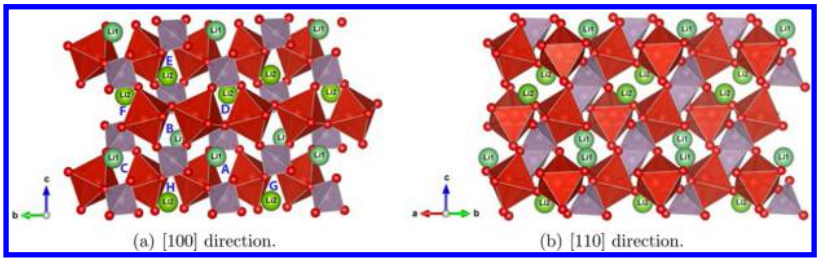

Figure 10. Crystallographically distinct Li in $LiVOPO_4$ and investigated diffusion paths in $LiVOPO_4$ viewed along (a) [100] and (b) [110] directions. A total of six different vacancy hops were investigated. Using the labeling scheme in (a), hops A → B and B → C form a 1D channel comprising only Li1 sites, whereas hops D → E and E → F form a similar 1D channel comprising only Li2 sites. In addition, hops from one 1D channel to another (hops A → G and A → H) were also investigated.

as shown in Figure 10. We investigated all hops between nearest neighbor Li sites (A → B, B → C, D → E, E → F, A → , G and A → H, see Figure 10a for labeling scheme). The results are shown in Figure 11.

For the 1D path A → B → C, both hops A → B and B → C involve the migration through the space between two VO_6 octahedra, resulting in fairly similar activation barriers of 244 and 214 meV respectively. For the 1D path D → E → F on the other hand, the migration local environments are extremely different for hops D → E and E → F. The D → E hop takes place through two VO_6 octahedra (similar to hops A → B and B → C), but the much smaller channel size results in a significantly higher migration barrier of 600 meV. Unlike the previous hops, the E → F hop passes through two PO_4 tetrahedra instead of VO_6 octahedra. In fact, the midpoint of E → F hop is found to be lower in energy than the end points, which we attribute to a reduction in the electrostatic repulsion between nearest neighbor Li^+ with the introduction of a vacancy. Overall, we find that the effective migration barriers (across the entirety of each path) for the Li1 (A → B → C) and Li2 (D → E → F) paths are 244 and 703 meV respectively. This suggests that v_{Li+} migration is likely to be relatively facile at least along the Li1 1D chains. Interchain vacancy migration barriers (A → G and A → H) are found to be significantly higher at 815 and 1199 meV.

We may estimate the diffusion coefficient D of $LiVOPO_4$ using transition-state theory as follows:

$$D = a^2 \times \upsilon \times \exp(-E_a/(k_B T)) \quad (1)$$

where a is the length of a diffusion jump, υ is the attempt frequency, E_a is the activation energy, and $k_B T$ is Boltzmann's constant times the temperature.[48] Using a typical phonon frequency of 10^{12} Hz, the diffusion coefficient at 300 K for $LiVOPO_4$ in the dilute limit is estimated to be 6.73×10^{-8} cm^2 s^{-1} (based on the lowest activation energy 1D channel), which is in relatively good agreement with the lithium chemical coefficient obtained from GITT or electrochemical impedance spectroscopy measurements (10^{-10} to 10^{-9} cm^2 s^{-1}).[9]

Electronic Conductivity. The calculated densities of states (DOSs) of Li_xVOPO_4 are shown in Figure 12. We find that all Li_xVOPO_4 phases have a fairly large band gap (2.25−2.99 eV), though the band gap decreases with increasing lithiation. The

DOI: 10.1021/acs.chemmater.5b04880
Chem. Mater. 2016, 28, 1794−1805

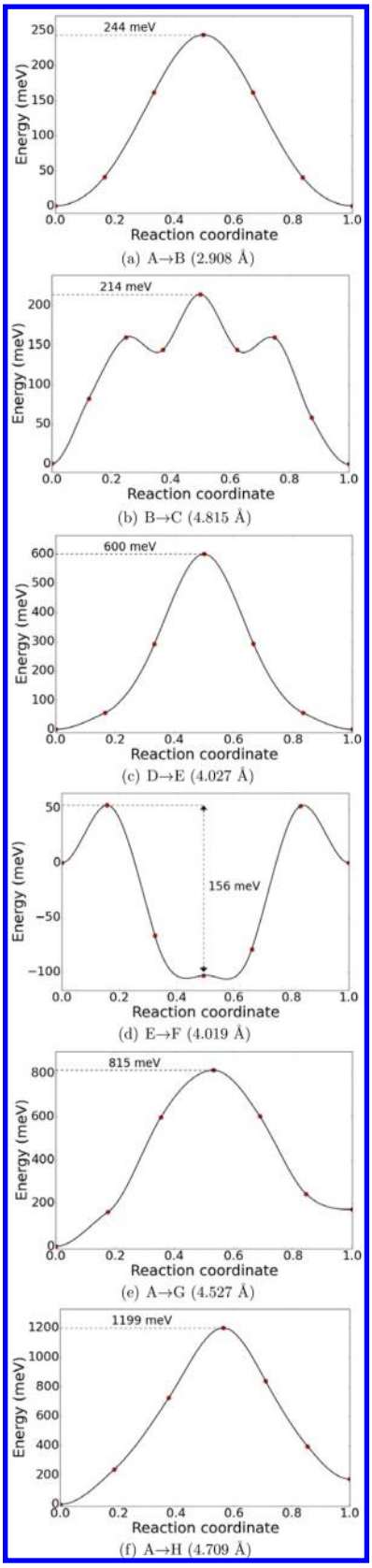

Figure 11. Calculated GGA CI-NEB migration barriers for various vacancy hops in $LiVOPO_4$.

calculated band gap of $LiVOPO_4$ (2.63 eV) is comparable with previous experimental measurements and theoretical calculations (2.13 and 2.78 eV respectively).[49]

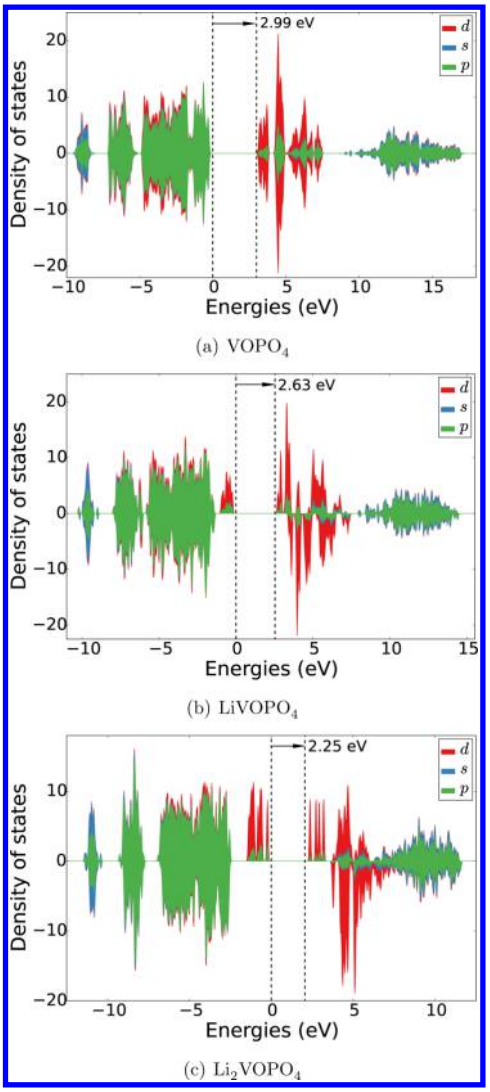

Figure 12. Orbital projected densities of states of Li_xVOPO_4 from HSE calculations.

Figure 13 summarizes the calculated migration barriers for the various polarons in Li_xVOPO_4 and provides a comparison to polaron migration barriers previously calculated for the olivine $LiFePO_4$ and $LiMnPO_4$ cathode materials[43] using the same computational methodology. In general, we find that the polaron migration barriers in the Li_xVOPO_4 to be higher than those in $LiFePO_4$ and comparable to those in $LiMnPO_4$.

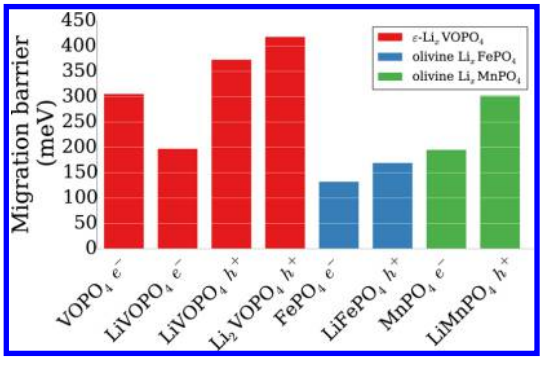

Figure 13. Comparison of calculated HSE polaron migration barriers for Li_xVOPO_4 with olivine $LiFePO_4$ and $LiMnPO_4$ from ref 43.

DOI: 10.1021/acs.chemmater.5b04880
Chem. Mater. 2016, 28, 1794−1805

DISCUSSION

ε-$VOPO_4$ is a highly promising cathode material due to its potential ability to intercalate two Li per vanadium to achieve a very high theoretical capacity of 318 mAh g^{-1}.[9,11,12,47] In contrast to previous efforts, we have demonstrated in this work the stable cycling of solid-state synthesized ε-$LiVOPO_4$ over more than one Li for more than 20 cycles. Furthermore, our combined DFT, operando PDF, and EXAFS analysis have yielded new insights into the thermodynamic and kinetic factors influencing the electrochemical performance in this material.

In general, the electrochemical performance obtained in this work is consistent with the earlier reports.[9,11,12,47] The discharge−charge profiles, with steps at ∼3.9, 2.5, 2.2, and 2.0 V, suggest the existence of intermediate phases at x = 1.5 and 1.75. It should be noted that there is some minor disagreement on the low voltage regime in the experimental literature. Although previous works[11,12,47] agree on the existence of an intermediate phase at x = 1.5, these works disagree on whether there is a second intermediate phase at x = 1.75,[12,47] or a solid solution regime for $1.5 \leq x \leq 2$.[11] Our results support the former findings, though the x = 1.75 phase is only slightly below the tie-line formed by the $Li_{1.5}VOPO_4$ and Li_2VOPO_4 phases.

From our electrochemical cycling data in Figure 2, we may make the observation that it is somewhat easier to intercalate Li into $LiVOPO_4$ than to remove Li from $LiVOPO_4$. However, intercalation of Li into $LiVOPO_4$ is associated with increasing polarization with cycling. Our results suggest that the limitation in extracting Li from $LiVOPO_4$ at high voltage is kinetic in nature, whereas the increasing polarization during intercalation at low voltage is probably due to thermodynamically driven structural changes.

From NEB calculations, we find that $LiVOPO_4$ is a pseudo-1D vacancy diffuser, with much lower effective migration barriers for the Li1 path (244 meV) than for the Li2 path (703 meV). The barriers for the Li1 path are also significantly lower than the Li migration barriers in the charged $VOPO_4$ material (463 meV) calculated by Mueller et al.[40] This suggests that (a) initial extraction of Li is likely to take place from the Li1 channel, and (b) there may be asymmetry in the kinetics between charge and discharge for $0 \leq x \leq 1$. This observation is consistent with the results of our GITT measurements, which find much lower overpotentials for high-voltage discharge compared to high-voltage charging. It could account for why full extraction of Li from $LiVOPO_4$ is difficult, as well as the larger polarization observed at the end of charge in most experiments.[9,10,12] It should be noted that the computed vacancy migration barriers in this work are different from those recently calculated by Ling et al.,[32] who concluded that vacancy migration in $LiVOPO_4$ follows a 2D network. However, as noted by the authors themselves, the relaxed $LiVOPO_4$ structure in Ling et al.'s[32] work shows significant deviation from the experimental structure, and their GGA+U NEB migration barriers are for a combination of ionic and electron migration.

The DFT calculations, PDF and EXAFS analysis provide strong evidence of thermodynamically driven structural changes during Li insertion into $LiVOPO_4$. First, the DFT calculated phase diagram show that the Li_xVOPO_4 phases are highly unstable for x > 1, with E_{hull} as high as 81 meV per atom for the Li_2VOPO_4 end member. Second, operando PDF and EXAFS data show evidence of a clear hysteresis in VO_6 local environments during low-voltage cycling. In particular, an irreversible increase in a V—O long bond at >2.4 Å is observed. The long V—O bond at >2.4 Å found in both PDF and EXAFS local structure analysis of the cycled samples, as well as in a previous EXAFS study by Allen et al.,[45] but it is not reflected in the VO_6 environments of the DFT-relaxed or experimentally derived Li_xVOPO_4 structures. VO_6 environments with a long V—O bond close to that observed (>2.3 Å) are known for $HVOPO_4$, which shares the same VO_6—PO_4 connectivity as ε-Li_xVOPO_4.[50] DFT relaxations of both $HVOPO_4$ and H_2VOPO_4 derived by substituting H for Li in $LiVOPO_4$ and Li_2VOPO_4, respectively, also show a significant extension in certain V—O bond lengths. Accordingly, we speculate that the observed >2.4 Å V—O bond is associated with H incorporation into the Li_xVOPO_4 structure, perhaps as a H/Li solid solution. Hydride formation is known to occur for V-based catalysts in organic solution.[51,52] Here, we believe the H likely results from electrolyte decomposition. A recent detailed study of the thermal stability of cathodes by some of the authors provides strong evidence that the charged $VOPO_4$ tends to oxidize the electrolyte to form H_xVOPO_4.[53] The structural distortions resulting from this H incorporation may provide an explanation for the increasing polarization during cycling. The investigation of this hypothesis will be the subject of future work.

The DFT results on the ionic and electronic conductivity in Li_xVOPO_4 emphasize the importance of nanosizing and carbon coating in achieving good electrochemical performance. The pseudo-1D nature of the diffusion pathways in Li_xVOPO_4 (this work and the work of Mueller et al.[40]), similar to the olivine Li_xMPO_4 cathodes,[54,55] makes nanosizing crucial for maintaining facile Li conduction, given the fact that inevitable channel blocking defects at the macroscopic limit would limit the conductivity in 1D diffusers.[56] We also find Li_xVOPO_4 to be a large band gap insulator throughout the entire lithiation range, and calculated polaron migration barriers are similar to those in the olivine $LiMPO_4$ systems. Therefore, carbon-coating and nanosizing are essential for electronic conductivity as well.[47,57−60] It should be noted that this result is contrary to the previous measurements of Song et al.,[9] who found $VOPO_4$ (10^{-6} S cm^{-1}) to have a much higher electronic conductivity compared to $LiFePO_4$ (10^{-8}−10^{-10} S cm^{-1}).[9,61,62] It is our wish that future experiments into the electronic conductivity across different states of charge, especially for the x = 1 and x = 2 end members, would be carried out to more conclusively verify the first-principles predictions and previous experimental results.

CONCLUSIONS

To conclude, we have demonstrated that solid-state synthesized $LiVOPO_4$ can be stably cycled over 1.65 Li for more than 20 cycles. About 65% of the theoretical capacity was achieved during delithiation from $LiVOPO_4$ to $VOPO_4$ in the high-voltage regime, whereas almost 100% of theoretical capacity was obtained during lithiation of $LiVOPO_4$ to Li_2VOPO_4 in the low-voltage regime, albeit with increasing polarization. Using a combination of DFT calculations, GITT measurements, operando PDF analysis and EXAFS spectra, we show that the capacity limitations during delithiation is likely to be driven by Li mobility limitations, whereas the increasing polarization during lithiation is the result of structural changes. We also show that Li_xVOPO_4 is likely to be a pseudo-1D ionic conductor with low electronic conductivity, for which nanosiz-

DOI: 10.1021/acs.chemmater.5b04880
Chem. Mater. 2016, 28, 1794−1805

ing and carbon coating is essential to achieve good electrochemical performance.

■ ASSOCIATED CONTENT

Supporting Information

The Supporting Information is available free of charge on the ACS Publications website at DOI: 10.1021/acs.chemmater.5b04880.

Details of experimental methods; computational methodology; comparison of DFT voltages with literature, predicted structures for $Li_{1.5}VOPO_4$ and $Li_{1.75}VOPO_4$; PDF structural models and refinement for Li_xVOPO_4; EXAFS analysis; bond lengths and density of states of polaronic structures. (PDF)

■ AUTHOR INFORMATION

Corresponding Authors

*E-mail: stanwhit@gmail.com.
*E-mail: chapmank@aps.anl.gov.
*E-mail: ongsp@eng.ucsd.edu.

Author Contributions

¶These authors contributed equally to this work.

Notes

These authors contribute equally to this work. Y.-C. Lin performed the DFT calculations; B. Wen developed the synthesis method, synthesized the materials, and performed initial X-ray diffraction characterization, electrochemical characterization; K. M. Wiaderek performed the synchrotron diffraction and operando pair distribution function measurements and data reduction.

■ ACKNOWLEDGMENTS

This research is supported as part of the NorthEast Center for Chemical Energy Storage (NECCES), an Energy Frontier Research Center funded by the U.S. Department of Energy, Office of Science, Office of Basic Energy Sciences under Award Number DE-SC0012583. We thank Drs. T. Wu and G. Sterbinsky for supporting experiments at 9-BM. This research used resources of the Advanced Photon Source, a U.S. Department of Energy (DOE) Office of Science User Facility operated for the DOE Office of Science by Argonne National Laboratory under Contract No. DE-AC02-06CH11357.

■ REFERENCES

(1) Whittingham, M. S. Electrical energy storage and intercalation chemistry. *Science* **1976**, *192*, 1126−1127.
(2) Whittingham, M. S. Intercalation and lattice expansion in titanium disulfide. *J. Chem. Phys.* **1975**, *62*, 1588.
(3) Mizushima, K.; Jones, P.; Wiseman, P.; Goodenough, J. LixCoO2 (0 < x ≤ 1): A new cathode material for batteries of high energy density. *Solid State Ionics* **1981**, *3*−*4*, 171−174.
(4) Padhi, A. K.; Nanjundaswamya, K.; Goodenough, J. Phospho-olivines as Positive-Electrode Materials for Rechargeable Lithium Batteries. *J. Electrochem. Soc.* **1997**, *144*, 1188.
(5) Whittingham, M. S. Ultimate limits to intercalation reactions for lithium batteries. *Chem. Rev.* **2014**, *114*, 11414−11443.
(6) Whittingham, M. S. History, Evolution, and Future Status of Energy Storage. *Proc. IEEE* **2012**, *100*, 1518−1534.
(7) Xu, K.; About, M.; Article, T. Nonaqueous Liquid Electrolytes for Lithium-Based Rechargeable Batteries. *Chem. Rev.* **2004**, *104*, 4303−4418.
(8) Hautier, G.; Jain, A.; Ong, S. P.; Kang, B.; Moore, C.; Doe, R.; Ceder, G. Phosphates as lithium-ion battery cathodes: An evaluation based on high-throughput ab initio calculations. *Chem. Mater.* **2011**, *23*, 3495−3508.
(9) Song, Y.; Zavalij, P. Y.; Whittingham, M. S. ϵ-VOPO[sub 4]: Electrochemical Synthesis and Enhanced Cathode Behavior. *J. Electrochem. Soc.* **2005**, *152*, A721.
(10) Chen, Z.; Chen, Q.; Chen, L.; Zhang, R.; Zhou, H.; Chernova, N. A.; Whittingham, M. S. Electrochemical Behavior of Nanostructured ϵ-VOPO4 over Two Redox Plateaus. *J. Electrochem. Soc.* **2013**, *160*, A1777−A1780.
(11) Harrison, K. L.; Bridges, C. a.; Segre, C. U.; Varnado, C. D.; Applestone, D.; Bielawski, C. W.; Paranthaman, M. P.; Manthiram, A. Chemical and electrochemical lithiation of LiVOPO4 cathodes for lithium-ion batteries. *Chem. Mater.* **2014**, *26*, 3849−3861.
(12) Bianchini, M.; Ateba-Mba, J. M.; Dagault, P.; Bogdan, E.; Carlier, D.; Suard, E.; Masquelier, C.; Croguennec, L. Multiple phases in the ϵ-VPO4O - LiVPO4O - Li2VPO4O system: a combined solid state electrochemistry and diffraction structural study. *J. Mater. Chem. A* **2014**, *2*, 10182.
(13) Kerr, T. A. Highly Reversible Li Insertion at 4 V in ϵ-VOPO4/α-LiVOPO4 Cathodes. *Electrochem. Solid-State Lett.* **1999**, *3*, 460.
(14) Borkiewicz, O. J.; Shyam, B.; Wiaderek, K. M.; Kurtz, C.; Chupas, P. J.; Chapman, K. W. The AMPIX electrochemical cell: a versatile apparatus for in situ X-ray scattering and spectroscopic measurements. *J. Appl. Crystallogr.* **2012**, *45*, 1261−1269.
(15) Chupas, P. J.; Qiu, X.; Hanson, J. C.; Lee, P. L.; Grey, C. P.; Billinge, S. J. Rapid-acquisition pair distribution function (RA-PDF) analysis. *J. Appl. Crystallogr.* **2003**, *36*, 1342−1347.
(16) Chupas, P. J.; Chapman, K. W.; Lee, P. L. Applications of an amorphous silicon-based area detector for high-resolution, high-sensitivity and fast time-resolved pair distribution function measurements. *J. Appl. Crystallogr.* **2007**, *40*, 463−470.
(17) Hammersley, A. P.; Svensson, S. O.; Hanfland, M.; Fitch, A. N.; Hausermann, D. Two-dimensional detector software: From real detector to idealised image or two-theta scan. *High Pressure Res.* **1996**, *14*, 235−248.
(18) Qiu, X.; Thompson, J. W.; Billinge, S. J. L. PDFgetX2: a GUI-driven program to obtain the pair distribution function from X-ray powder diffraction data. *J. Appl. Crystallogr.* **2004**, *37*, 678−678.
(19) Farrow, C. L.; Juhas, P.; Liu, J. W.; Bryndin, D.; Božin, E. S.; Bloch, J.; Proffen, T.; Billinge, S. J. L. PDFfit2 and PDFgui: computer programs for studying nanostructure in crystals. *J. Phys.: Condens. Matter* **2007**, *19*, 335219.
(20) Wojdyr, M. Fityk: a general-purpose peak fitting program. *J. Appl. Crystallogr.* **2010**, *43*, 1126−1128.
(21) Ravel, B.; Newville, M. ATHENA, ARTEMIS, HEPHAESTUS: data analysis for X-ray absorption spectroscopy using IFEFFIT. *J. Synchrotron Radiat.* **2005**, *12*, 537−541.
(22) Kresse, G. Efficient iterative schemes for ab initio total-energy calculations using a plane-wave basis set. *Phys. Rev. B: Condens. Matter Mater. Phys.* **1996**, *54*, 11169−11186.
(23) Blochl, P. E. Projector augmented-wave method. *Phys. Rev. B: Condens. Matter Mater. Phys.* **1994**, *50*, 17953−17979.
(24) Bergerhoff, G.; Hundt, R.; Sievers, R.; Brown, I. D. The inorganic crystal structure data base. *J. Chem. Inf. Model.* **1983**, *23*, 66−69.
(25) Hart, G. L. W.; Forcade, R. W. Algorithm for generating derivative structures. *Phys. Rev. B: Condens. Matter Mater. Phys.* **2008**, *77*, 1−12.
(26) Ong, S. P.; Richards, W. D.; Jain, A.; Hautier, G.; Kocher, M.; Cholia, S.; Gunter, D.; Chevrier, V. L.; Persson, K. a.; Ceder, G. Python Materials Genomics (pymatgen): A robust, open-source python library for materials analysis. *Comput. Mater. Sci.* **2013**, *68*, 314−319.
(27) Perdew, J. P.; Burke, K.; Ernzerhof, M. Generalized Gradient Approximation Made Simple. *Phys. Rev. Lett.* **1996**, *77*, 3865−3868.
(28) Anisimov, V. I.; Aryasetiawan, F.; Lichtenstein, a. I. First-principles calculations of the electronic structure and spectra of strongly correlated systems: The LDA+U method. *J. Phys.: Condens. Matter* **1997**, *9*, 767−808.

DOI: 10.1021/acs.chemmater.5b04880
Chem. Mater. 2016, 28, 1794−1805

(29) Liechtenstein, A. I.; Anisimov, V. I.; Zaanen, J. Density-functional theory and strong interactions: Orbital ordering in Mott-Hubbard insulators. *Phys. Rev. B: Condens. Matter Mater. Phys.* **1995**, *52*, R5467−R5470.
(30) Dudarev, S. L.; Savrasov, S. Y.; Humphreys, C. J.; Sutton, a. P.; Botton, G. A. Electron-energy-loss spectra and the structural stability of nickel oxide: An LSDA+U study. *Phys. Rev. B: Condens. Matter Mater. Phys.* **1998**, *57*, 1505−1509.
(31) Jain, A.; Ong, S. P.; Hautier, G.; Chen, W.; Richards, W. D.; Dacek, S.; Cholia, S.; Gunter, D.; Skinner, D.; Ceder, G.; Persson, K. A. Commentary: The materials project: A materials genome approach to accelerating materials innovation. *APL Mater.* **2013**, *1*, 011002.
(32) Ling, C.; Zhang, R.; Mizuno, F. Phase stability and its impact on the electrochemical performance of VOPO 4 and LiVOPO 4. *J. Mater. Chem. A* **2014**, *2*, 12330.
(33) Ong, S. P.; Wang, L.; Kang, B.; Ceder, G. $LiFePO_2$ Phase Diagram from First Principles Calculations. *Chem. Mater.* **2008**, *20*, 1798−1807.
(34) Ong, S. P.; Cholia, S.; Jain, A.; Brafman, M.; Gunter, D.; Ceder, G.; Persson, K. a. The Materials Application Programming Interface (API): A simple, flexible and efficient API for materials data based on REpresentational State Transfer (REST) principles. *Comput. Mater. Sci.* **2015**, *97*, 209−215.
(35) Aydinol, M.; Kohan, a.; Ceder, G.; Cho, K.; Joannopoulos, J. Ab initio study of lithium intercalation in metal oxides and metal dichalcogenides. *Phys. Rev. B: Condens. Matter Mater. Phys.* **1997**, *56*, 1354−1365.
(36) Heyd, J.; Scuseria, G. E.; Ernzerhof, M. Hybrid functionals based on a screened Coulomb potential. *J. Chem. Phys.* **2003**, *118*, 8207−8215.
(37) Heyd, J.; Scuseria, G. E.; Ernzerhof, M. Erratum: "Hybrid functionals based on a screened Coulomb potential" [J. Chem. Phys. 118, 8207 (2003)]. *J. Chem. Phys.* **2006**, *124*, 219906.
(38) Henkelman, G.; Uberuaga, B. P.; Jónsson, H. Climbing image nudged elastic band method for finding saddle points and minimum energy paths. *J. Chem. Phys.* **2000**, *113*, 9901−9904.
(39) Henkelman, G.; Jónsson, H. Improved tangent estimate in the nudged elastic band method for finding minimum energy paths and saddle points. *J. Chem. Phys.* **2000**, *113*, 9978−9985.
(40) Mueller, T.; Hautier, G.; Jain, A.; Ceder, G. Evaluation of tavorite-structured cathode materials for lithium-ion batteries using high-throughput computing. *Chem. Mater.* **2011**, *23*, 3854−3862.
(41) Heyd, J.; Scuseria, G. E. Efficient hybrid density functional calculations in solids: Assessment of the Heyd-Scuseria-Ernzerhof screened Coulomb hybrid functional. *J. Chem. Phys.* **2004**, *121*, 1187−1192.
(42) Henderson, T. M.; Paier, J.; Scuseria, G. E. Accurate treatment of solids with the HSE screened hybrid. *Phys. Status Solidi B* **2011**, *248*, 767−774.
(43) Ong, S. P.; Chevrier, V. L.; Ceder, G. Comparison of small polaron migration and phase separation in olivine LiMnPO4 and LiFePO4 using hybrid density functional theory. *Phys. Rev. B: Condens. Matter Mater. Phys.* **2011**, *83*, 075112.
(44) Ateba Mba, J.-M.; Masquelier, C.; Suard, E.; Croguennec, L. Synthesis and Crystallographic Study of Homeotypic LiVPO4F and LiVPO4O. *Chem. Mater.* **2012**, *24*, 1223−1234.
(45) Allen, C. J.; Jia, Q.; Chinnasamy, C. N.; Mukerjee, S.; Abraham, K. M. Synthesis, Structure and Electrochemistry of Lithium Vanadium Phosphate Cathode Materials. *J. Electrochem. Soc.* **2011**, *158*, A1250.
(46) Quackenbush, N. F.; Wangoh, L.; Scanlon, D. O.; Zhang, R.; Chung, Y.; Chen, Z.; Wen, B.; Lin, Y.; Woicik, J. C.; Chernova, N. A.; Ong, S. P.; Whittingham, M. S.; Piper, L. F. J. Interfacial effects in ϵ-Li x $VOPO_4$ and evolution of the electronic structure. *Chem. Mater.* **2015**, *27*, 8211.
(47) Chen, Z.; Ren, Y.; Jansen, A. N.; Lin, C.-K.; Weng, W.; Amine, K. New class of nonaqueous electrolytes for long-life and safe lithium-ion batteries. *Nat. Commun.* **2013**, *4*, 1513.
(48) Vineyard, G. H. Frequency factors and isotope effects in solid state rate processes. *J. Phys. Chem. Solids* **1957**, *3*, 121−127.
(49) Yang, Y.; Fang, H.; Zheng, J.; Li, L.; Li, G.; Yan, G. Towards the understanding of poor electrochemical activity of triclinic LiVOPO4: Experimental characterization and theoretical investigations. *Solid State Sci.* **2008**, *10*, 1292−1298.
(50) Wilde, L.; Trommer, J.; Steinike, U.; Worzala, H.; Wolf, G.-U. Ab initio Structure Analysis of VO(HPO4). *Mater. Sci. Forum* **1998**, *278−281*, 704−707.
(51) Cabello Sanchez, F. J.; Lopez-Sanchez, J. A.; Wells, R. P.; Rhodes, C.; Isfahani, A.-Z.; Hutchings, G. Effect of Dehydration of VOPO42H2O on the Preparation and Reactivity of Vanadium Phosphate Catalyst for the Oxidation of n-Butane. *Catal. Lett.* **2001**, *77*, 189−192.
(52) Hutchings, G. J. Vanadium phosphate: a new look at the active components of catalysts for the oxidation of butane to maleic anhydride. *J. Mater. Chem.* **2004**, *14*, 3385.
(53) Huang, Y.; Lin, Y.-C.; Jenkins, D. M.; Chernova, N. A.; Chung, Y.; Radhakrishnan, B.; Chu, I.-H.; Fang, J.; Wang, Q.; Omenya, F.; Ong, S. P.; Whittingham, M. S. Thermal stability and reactivity of cathode materials for Li-ion batteries. *ACS Appl. Mater. Interfaces* **2016**.
(54) Morgan, D.; Van der Ven, A.; Ceder, G. Li Conductivity in $LixMPO_4$ (M = Mn, Fe, Co, Ni) Olivine Materials. *Electrochem. Solid-State Lett.* **2004**, *7*, A30.
(55) Islam, M. S.; Driscoll, D. J.; Fisher, C. a. J.; Slater, P. R. Atomic-scale investigation of defects, dopants, and lithium transport in the LiFePO4 olivine-type battery material. *Chem. Mater.* **2005**, *17*, 5085−5092.
(56) Malik, R.; Burch, D.; Bazant, M.; Ceder, G. Particle size dependence of the ionic diffusivity. *Nano Lett.* **2010**, *10*, 4123−4127.
(57) Paul, B. J.; Mathew, V.; Do, G. X.; Kang, J.-W.; Gim, J.; Rai, a. K.; Singh, N. K.; Song, J.; Kim, J. Enhanced Storage Capacities in Carbon-Coated Triclinic-LiVOPO4 Cathode with Porous Structure for Li-Ion Batteries. *ECS Electrochem. Lett.* **2012**, *1*, A63−A65.
(58) Saravanan, K.; Lee, H. S.; Kuezma, M.; Vittal, J. J.; Balaya, P. Hollow α-LiVOPO4 sphere cathodes for high energy Li-ion battery application. *J. Mater. Chem.* **2011**, *21*, 10042.
(59) Li, H.; Zhou, H. Enhancing the performances of Li-ion batteries by carbon-coating: present and future. *Chem. Commun.* **2012**, *48*, 1201−1217.
(60) Lee, K. T.; Cho, J. Roles of nanosize in lithium reactive nanomaterials for lithium ion batteries. *Nano Today* **2011**, *6*, 28−41.
(61) Chung, S.-Y.; Bloking, J. T.; Chiang, Y.-M. Electronically conductive phospho-olivines as lithium storage electrodes. *Nat. Mater.* **2002**, *1*, 123−128.
(62) Xu, Y.-N.; Chung, S.-Y.; Bloking, J. T.; Chiang, Y.-M.; Ching, W. Y. Electronic Structure and Electrical Conductivity of Undoped LiFePO4. *Electrochem. Solid-State Lett.* **2004**, *7*, A131.

DOI: 10.1021/acs.chemmater.5b04880
Chem. Mater. 2016, 28, 1794−1805